UC Riverside
UC Riverside Previously Published Works

Title
Unravelling the Stability and Capsid Dynamics of the Three Virions of Brome Mosaic Virus Assembled Autonomously In Vivo.

Authors
Chakravarty, Antara
Reddy, Vijay S
Rao, ALN

Unravelling the Stability and Capsid Dynamics of the Three Virions of Brome Mosaic Virus Assembled Autonomously *In Vivo*

Antara Chakravarty,[a] Vijay S. Reddy,[b] A. L. N. Rao[a]

[a]Department of Microbiology and Plant Pathology, University of California, Riverside, Riverside, California, USA
[b]Department of Integrative Structural and Computational Biology, The Scripps Research Institute, La Jolla, California, USA

ABSTRACT Viral capsids are dynamic assemblies that undergo controlled conformational transitions to perform various biological functions. The replication-derived four-molecule RNA progeny of *Brome mosaic virus* (BMV) is packaged by a single capsid protein (CP) into three types of morphologically indistinguishable icosahedral virions with T=3 quasisymmetry. Type 1 (B1^V) and type 2 (B2^V) virions package genomic RNA1 and RNA2, respectively, while type 3 (B3+4^V) virions copackage genomic RNA3 (B3) and its subgenomic RNA4 (sgB4). In this study, the application of a robust *Agrobacterium*-mediated transient expression system allowed us to assemble each virion type separately *in planta*. Experimental approaches analyzing the morphology, size, and electrophoretic mobility failed to distinguish between the virion types. Thermal denaturation analysis and protease-based peptide mass mapping experiments were used to analyze stability and the conformational dynamics of the individual virions, respectively. The crystallographic structure of the BMV capsid shows four trypsin cleavage sites (K^{65}, R^{103}, K^{111}, and K^{165} on the CP subunits) exposed on the exterior of the capsid. Irrespective of the digestion time, while retaining their capsid structural integrity, B1^V and B2^V released a single peptide encompassing amino acids 2 to 8 of the N-proximal arginine-rich RNA binding motif. In contrast, B3+4^V capsids were unstable with trypsin, releasing several peptides in addition to the peptides encompassing four predicted sites exposed on the capsid exterior. These results, demonstrating qualitatively different dynamics for the three types of BMV virions, suggest that the different RNA genes they contain may have different translational timing and efficiency and may even impart different structures to their capsids.

IMPORTANCE The majority of viruses contain RNA genomes protected by a shell of capsid proteins. Although crystallographic studies show that viral capsids are static structures, accumulating evidence suggests that, in solution, virions are highly dynamic assemblies. The three genomic RNAs (RNA1, -2, and -3) and a single subgenomic RNA (RNA4) of Brome mosaic virus (BMV), an RNA virus pathogenic to plants, are distributed among three physically homogeneous virions. This study examines the thermal stability by differential scanning fluorimetry (DSF) and capsid dynamics by matrix-assisted laser desorption ionization–time of flight (MALDI-TOF) analyses following trypsin digestion of the three virions assembled separately *in vivo* using the *Agrobacterium*-mediated transient expression approach. The results provide compelling evidence that virions packaging genomic RNA1 and -2 are distinct from those copackaging RNA3 and -4 in their stability and dynamics, suggesting that RNA-dependent capsid dynamics play an important biological role in the viral life cycle.

KEYWORDS capsid dynamics, stability, genome packaging, RNA virus, MALDI-TOF

Assembly of infectious virions is an essential step in the life cycle of RNA viruses pathogenic to eukaryotic organisms (1–3). Once assembled, a virion must fulfill two stringent requirements. First, it must be stable enough to withstand physicochemical aggression in the extracellular environment. Second, it must be flexible enough to release the viral genome in the host cell for subsequent replication. In order to meet these two competing demands, virions undergo dynamical fluctuations leading to biologically relevant surface conformational changes.

Brome mosaic virus (BMV), a prototype of the plant virus family *Bromoviridae*, ranks among the best-studied multipartite, positive-sense RNA viruses with respect to replication, virus assembly, and genome packaging (4, 5). The genome of BMV is divided among three RNAs: the largest two genomic RNAs of BMV, RNA1 (B1) and RNA2 (B2), are monocistronic, encoding nonstructural replicase proteins 1a (p1a) and 2a (p2a), respectively (6). The third genomic RNA, RNA3 (B3), is dicistronic, encoding at its 5′ end a nonstructural movement protein (MP) and at its 3′ end a structural capsid protein (CP) (6). CP is translated from a replication-derived subgenomic RNA4 (sgB4), which is synthesized from a minus-strand B3 by an internal initiation mechanism (7). A single CP packages the three genomic RNAs (B1, B2, and B3) and the one subgenomic RNA (sgB4) into three types of morphologically indistinguishable icosahedral virions (2, 6). Genomic RNAs B1 and B2 are packaged separately into two virion types, $B1^V$ and $B2^V$, respectively, while genomic B3 and sgB4 are copackaged into a third virion type, $B3+4^V$. Remarkably, all three virion types are physically homogeneous in size and morphology and are partially resolved by buoyant density sedimentation (8).

The structure of the BMV virion has been determined at 3.4-Å resolution showing a T=3 icosahedral symmetric capsid composed of 180 identical subunits of a single 20-kDa CP (9) (Fig. 1A). In the BMV virion, pentameric capsid protein subunit A contains ordered amino acid (aa) residues 41 to 189, while hexameric subunits B and C contain residues 25 to 189 and 1 to 189, respectively (9) (Fig. 1A). The first N-proximal 25-aa region of BMV CP contains an arginine-rich motif (ARM) and is not visible in the electron density map, since the N-ARM is disordered and interacts with RNA inside the capsid (9).

In addition to protecting the progeny RNA from the cellular environment, virion assembly in BMV is intimately associated with other functions such as modification of endoplasmic reticulum (ER) (10), symptom expression (11), and cell-to-cell spread (12). Therefore, it is reasonable to assume that all three virion types should exhibit physical and structural homogeneity to promote optimal interaction with the host machinery for establishing a successful infection in a given host system. Since the three virions of BMV are physically inseparable, the reported crystallographic structure of BMV virions (9) is an average of the three virion types. Therefore, it is not known whether the three virion types are structurally identical and how local and global dynamical conformational changes of the stable states of the viral capsids modulate functions of biological relevance. Thus, it is imperative to obtain, in pure form, each virion type, free from the remaining two counterparts. A previous attempt to separate each virion type using $CsCl_2$ buoyant density centrifugation has resulted in samples that are enriched in one type of virion but not free from the remaining two virion types (13, 14).

To understand the mechanism of RNA packaging and virion assembly in BMV, we have developed an *Agrobacterium*-mediated transient expression (agroinfiltration) system amenable for dissecting events involving RNA replication and packaging (15–17). A series of agroinfiltration experiments performed in the last decade revealed that although BMV RNA packaging is independent of replication, coexpression of viral replicase components enhances packaging specificity (16). Also, a physical interaction between CP and viral replicase, more specifically, replicase protein 2a, is obligatory in regulating RNA packaging specificity (18). Based on this collective information, in this study, we report a facile and robust agroinfiltration approach to separately assemble each virion type of BMV *in planta*. Further characterization of each virion type with respect to physical morphology by negative-stain electron microscopy (EM) and electrophoretic mobility profiles revealed that all three virion types are remarkably indistinguishable. However, examination of the viral surface structure using matrix-assisted
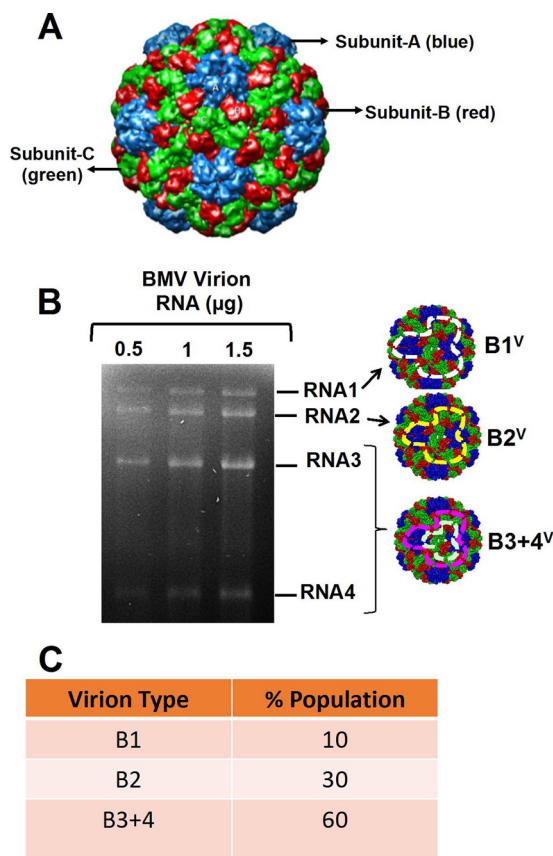
FIG 1 Quantitative analysis of the three types of BMV virions. (A) Structure of a BMV virion showing the arrangement of subunits A, B, and C. (B) RNA was isolated from wt purified virion preparation, denatured with formamide/formaldehyde, and subjected to 1.2% agarose gel electrophoresis as described previously. After staining with ethidium bromide, the amount of RNA molecules present in each band was estimated using ImageJ software (42). Three lanes, each containing a different total mass of RNA (0.5, 1, or 1.5 μg), were analyzed. (C) The intensity of each RNA band shown in panel B was determined using ImageJ (42) and was used to determine the mole ratios of the viral RNAs isolated from virions. These mole ratios were then used to determine the fraction of each virion type.

laser desorption ionization–time of flight (MALDI-TOF) mass spectrometry, an approach that can identify viral proteolysis products to examine the viral surface structure (19), revealed that virions of type 1 and 2 are dynamically distinct from those of type 3. The biological significance of the observed variation in the dynamics of the three different virions of BMV is discussed.

RESULTS

Throughout this study, virion types B1^V, B2^V, and B3+4^V represent individual virions packaging genomic RNA1, RNA2, and RNA3 plus -4, respectively. Wild type (wt) represents a constellation of three virions of BMV, each containing RNA1, RNA2, and RNA3 plus -4 purified from infected barley or *Nicotiana benthamiana* plants.

Determining the quantitative distribution of virion types in wt BMV. To estimate the percent distribution of each virion type, RNA was isolated from purified wt virions and subjected to denaturing agarose gel electrophoresis. Following ethidium bromide staining, the percent distribution of each of the four RNAs was estimated using ImageJ analysis (Fig. 1B). The results (an average from three independent assays) show that the three virion types accumulated disproportionately, with the most prevalent species (~60%) being virion type 3 that copackaged RNA3 plus -4, followed by virion type 2 packaging RNA2 (~30%), and virion type 1 packaging RNA1 (~10%) (Fig. 1C). Consequently, without separating each virion type—as described below—the mixed
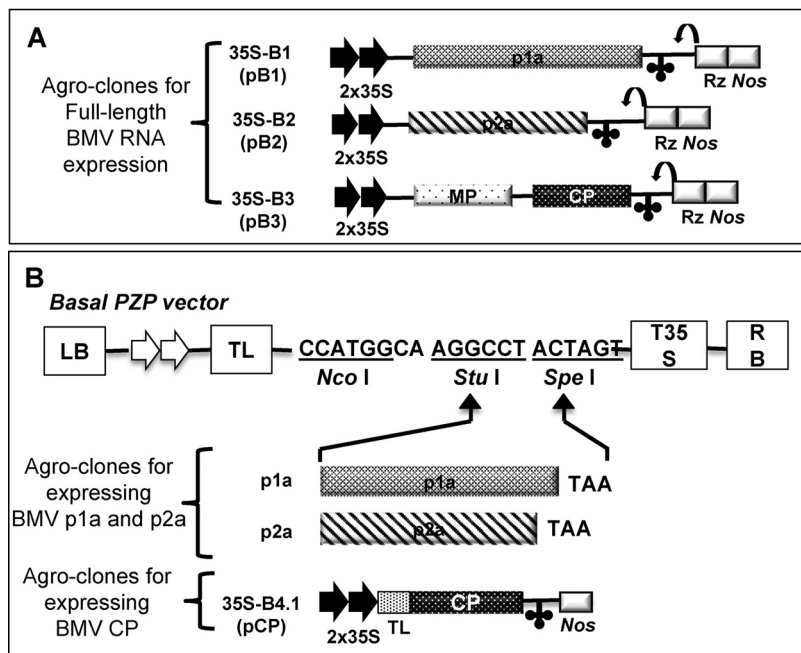
FIG 2 Characteristic features of agroplasmids used in this study. (A) Characteristics of agroplasmids harboring BMV genomic RNAs used for transient expression in plants. The 35S-B1 (pB1), 35S-B2 (pB2), and 35S-B3 (pB3) constructs contain full-length cDNA copies of BMV genomic RNA1 (B1), -2 (B2), and -3 (B3), respectively. Single lines and open boxes represent noncoding and coding regions, respectively. Monocistronic B1 encoding replicase protein 1a (p1a), and monocistronic B2 encoding replicase protein 2a (p2a) are indicated. In B3, the locations of the movement protein (MP) and coat protein (CP) genes are shown. At the 3' end of each construct, the clover leaf-like conformation represents a tRNA-like motif conserved among all three BMV genomic RNAs. Two black arrows at the 5' ends represent the double 35-S. A bent arrow indicates the predicted self-cleavage site by the ribozyme. The location of the *Nos* terminator is also indicated. (B) Agroconstructs for transient expression of p1a, p2a, and CP (pCP). Open reading frames (ORFs) of BMV p1a, p2a, and CP were fused in-frame to each pair of binary vectors using StuI and SpeI sites. Each binary vector contained, in sequential order, a left border of T-DNA (LB), a double 35S promoter (35S×2), a tobacco etch virus (TEV) translation enhancer leader sequence (TL), multiple cloning sites, a 35S terminator (T35S), and a right border of T-DNA (RB). The construction and characteristic features of pCP are as described previously (15).

nature of BMV virions obscures the interpretation of biochemical (13, 14) and structural studies (9).

Strategy for *in vivo* assembly of three independent virion types of BMV. Figure 2 summarizes the characteristic features of transfer DNA (T-DNA)-based vectors designed to express the three biologically active genomic RNAs (gRNAs) of BMV (pB1, pB2, and pB3) when transiently expressed in *N. benthamiana* plants (15). Likewise, T-DNA constructs shown in Fig. 2B are designed to transiently express BMV replicase proteins 1a (p1a), 2a (p2a), and CP (pCP). A strategy for the separate assembly of each virion type of BMV is shown schematically in Fig. 3. Prior to designing this strategy, we considered the following three criteria: first, genome packaging in BMV is functionally coupled to replication (16, 17), i.e., only the replication-derived progeny RNA is packaged into virions; second, BMV CP (BCP) expressed in the absence of replication is nonspecific in RNA packaging (15); third, the packaging specificity is dictated by an interaction between CP and p2a (18). Therefore, keeping these requirements in perspective, the strategy shown in Fig. 3 was designed to assemble desired virion types by infiltrating the following sets of inocula. (i) Agrotransformants of all three wild type (wt) plasmids (Fig. 3A) or only pCP (Fig. 3B) infiltrated into plants served as controls. (ii) An inoculum was formulated to assemble B1^V by mixing agrotransformants pB1, p2a, and pCP (Fig. 3C). Following infiltration into *N. benthamiana* leaves, pB1 would result in the synthesis of a biologically active full-length B1, and its translation would yield p1a. Agrotransformant p2a would result in the synthesis of an mRNA competent to translate p2a, but
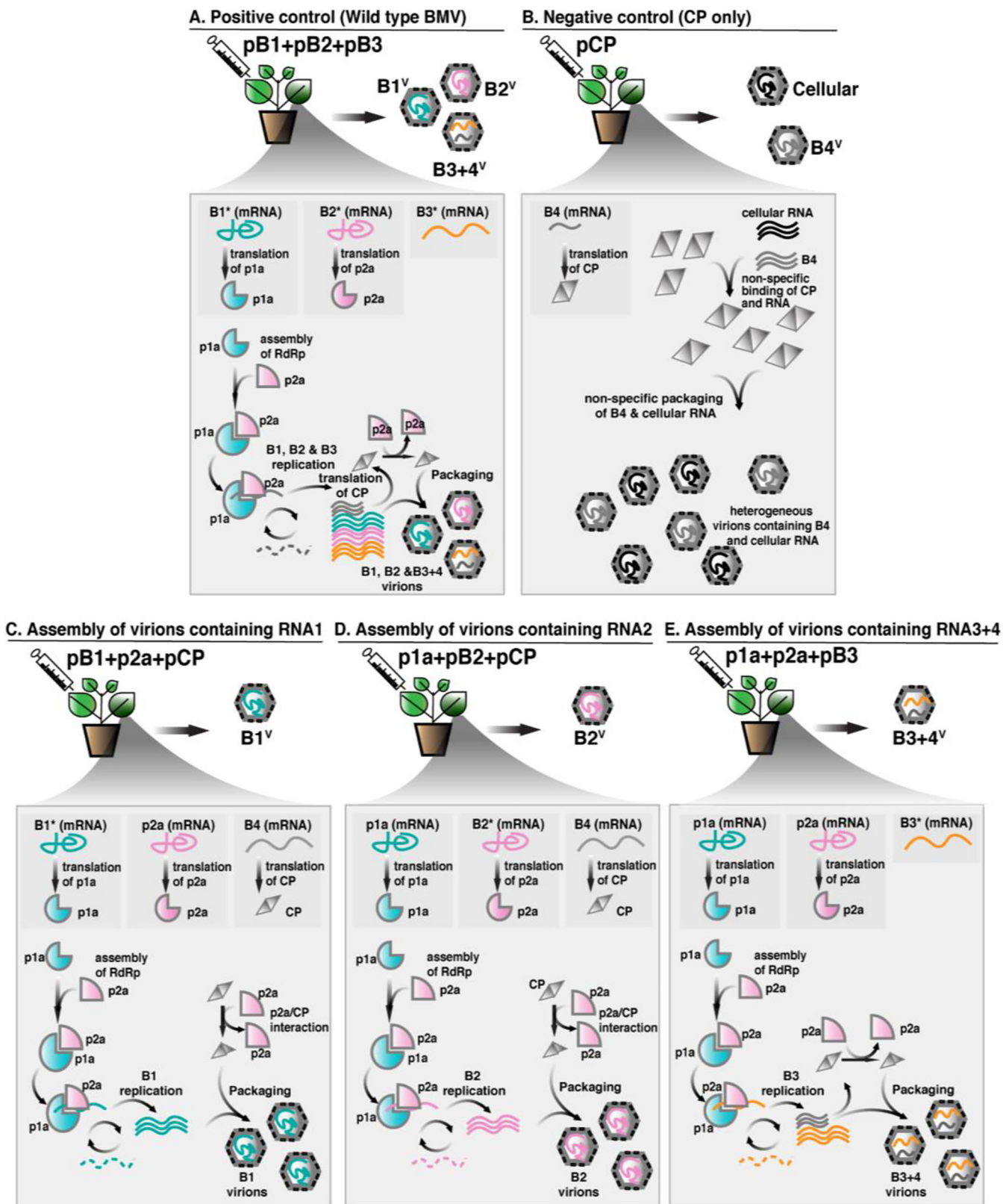
FIG 3 Schematic representation of the strategy used for autonomous assembly of the three virions of the BMV *in vivo*. (A) (Positive control) Infiltration of the inoculum containing a mixture of pB1+pB2+pB3 would induce wt BMV infection resulting in the assembly of mixture of all three virions; (B) (Negative control) Infiltration of the inoculum containing pCP would result in the expression of CP mRNA followed by the translation wt CP and nonspecific assembly of virions containing CP mRNA and cellular RNA, as demonstrated previously (15). (C) Assembly of virions packaging RNA1 (B1^V). A mixture of inoculum containing agrotransformants B1+p2a+pCP (see Fig. 2 for details) is infiltrated into *N. benthamiana* leaves. Transcription of pB1 results in the synthesis of a biologically

(Continued on next page)

it would not be replicated since it lacks 5′ and 3′ noncoding regions (Fig. 2B). Translation of mRNA synthesized from agrotransformant pCP would provide CP subunits to direct virion assembly. A functional replicase assembled with p1a and p2a would result in the replication of B1. Since replicase-CP interaction directs the packaging of replication-derived progeny (18), an interaction between p2a and CP would result in the assembly of B1^V (Fig. 3C). (iii) A similar strategy was used to assemble B2^V by mixing agrotransformants p1a, B2, and pCP (Fig. 3D). Infiltration would result in the synthesis of biologically active B2 and its translation product, i.e., p2a complexed with transiently expressed p1a would result in the assembly of a functional replicase followed by the assembly of B2^V (Fig. 3D). (iv) Finally, to assemble B3+4^V (copackaging B3 and sgB4), plants were infiltrated with a mixture of agrotransformants containing p1a, p2a, and B3 (Fig. 3E). Assembly of a functional replicase would result in the replication of B3 followed by the synthesis of sgB4 for CP production, resulting in the assembly of B3+4^V (Fig. 3E).

Characteristic properties of B1^V, B2^V, and B3+4^V. Sucrose density gradient-purified virions from *N. benthamiana* leaves infiltrated with either control infiltrations of wt (i.e., pB1+pB2+pB3) (Fig. 3A) or pCP (Fig. 3B) or with pB1+p2a+pBCP (i.e., B1^V) (Fig. 3C), p1a+pB2+pBCP (i.e., B2^V) (Fig. 3D), or p1a+p2a+pB3 (i.e., B3+4^V) (Fig. 3E) were subjected to negative-stain EM examination. Results shown in Fig. 4A indicate that virions of B1^V, B2^V, and B3+4^V are indistinguishable from those of the wt control in morphology and size (i.e., the average diameter being 26 to 28 nm). However, it is interesting to note that virions of B1^V appear to be fuller than those of B2^V and B3+4^V. It is likely that the interaction between the CP and large size of RNA1 (3.2 kb) compared to that of RNA2 (2.8 kb) or RNA3 plus -4 (2.9 kb) would result in the assembly of fuller particles. Additional experiments using cryo-EM are in progress to confirm this assumption.

The analysis of agarose gel electrophoretic mobility patterns of purified virions is an ideal approach for identifying changes, if any, in surface charge (20, 21). Therefore, B1^V, B2^V, and B3+4^V were subjected to agarose gel electrophoresis along with wt virions of BMV and *Cowpea Chlorotic Mottle virus* (CCMV; a member of the genus *Bromovirus*) as controls. The capsid sizes of BMV and CCMV are essentially identical (8). However, the charge on the solvent-accessible residues of BMV specified in VIPER (http://viperdb.scripps.edu/) is +1,020 compared to −1,209 for CCMV. Consequently, CCMV and BMV migrate toward the positive and negative electrodes, respectively (22). Results shown in Fig. 4B confirmed the relative electrophoretic mobilities of wt BMV and CCMV virions (Fig. 4B, compare lanes 1 and 2). The indistinguishable electrophoretic mobility profiles of wt BMV (Fig. 4B, lane 2) and either B1^V (Fig. 4B, lane 3), B2^V (Fig. 4B, lane 4), or B3+4^V (Fig. 4B, lane 5) suggest that all three virion types exhibit similar surface charges.

To confirm the genetic composition of B1^V, B2^V, and B3+4^V, virion RNA was isolated and subjected to a reverse transcription-PCR (RT-PCR) assay using a set of primers that are designed to specifically amplify each of the three gRNAs and a single sgRNA (see Materials and Methods). RNA isolated from wt virions was used as a control. Results shown in Fig. 5A confirmed that B1^V, B2^V, and B3+4^V encapsidated expected RNA progeny. Since the sgB4 RNA sequence is present in the 3′ half of B3, an additional Northern blot assay was used to confirm the copackaging of B3+4^V (data not shown).

To further assess the purity of B1^V, B2^V, and B3+4^V, an infectivity assay was performed in *Chenopodium quinoa*. As shown in Fig. 5B, phenotypic local and systemic

FIG 3 Legend (Continued)

active full-length genomic RNA1 whose translation gives functional replicase protein p1a; similarly, agrotransformant p2a results in an mRNA competent to give replicase p2a but not competent to be replicated, because it lacks the requisite 5′ and 3′ noncoding regions. Finally, translation of the mRNA transcribed from agrotransformant pCP gives the CP subunits for directing virion assembly. As a result, a functional replicase complex is assembled from proteins p1a and p2a that ensures the replication of B1 RNA followed by its packaging into virions by the transiently expressed CP subunits. (D) Assembly of virions packaging RNA2 (B2^V). The inoculum shown in this panel is identical to the one shown in panel A, except that pB1 and p2a are replaced by p1a and pB2, respectively. Agroinfiltration of this inoculum results in the assembly of virions containing B2 RNA. (E) Assembly of virions packaging RNA3 and -4 (B3+4^V). The inoculum shown in this panel is formulated to assemble virions packaging B3 RNA and sgB4 by mixing agrotransformants of p1a, p2a, and pB3. Transiently expressed proteins p1a and p2a then direct replication of B3 followed by the synthesis of sgB4 for CP production.
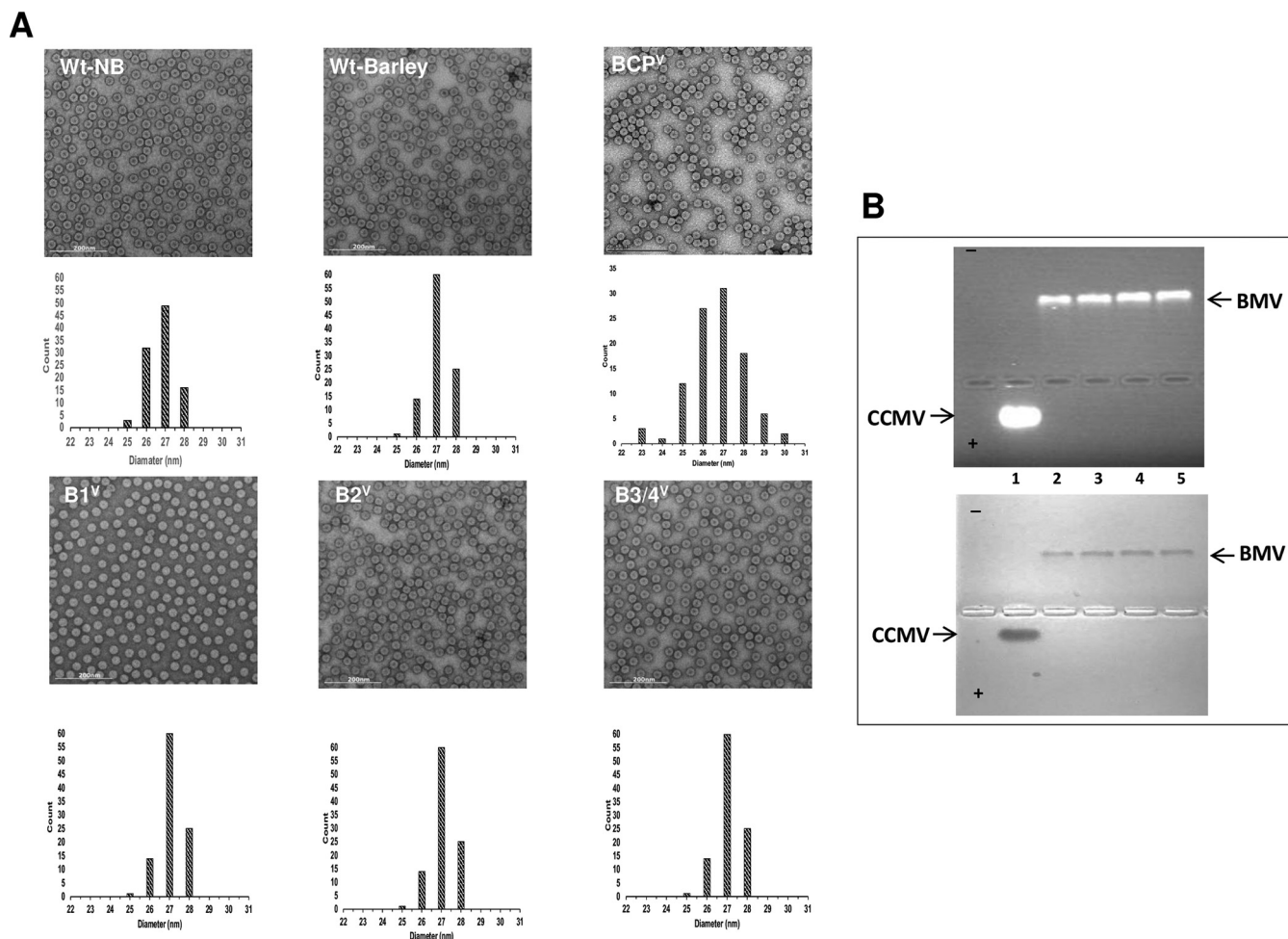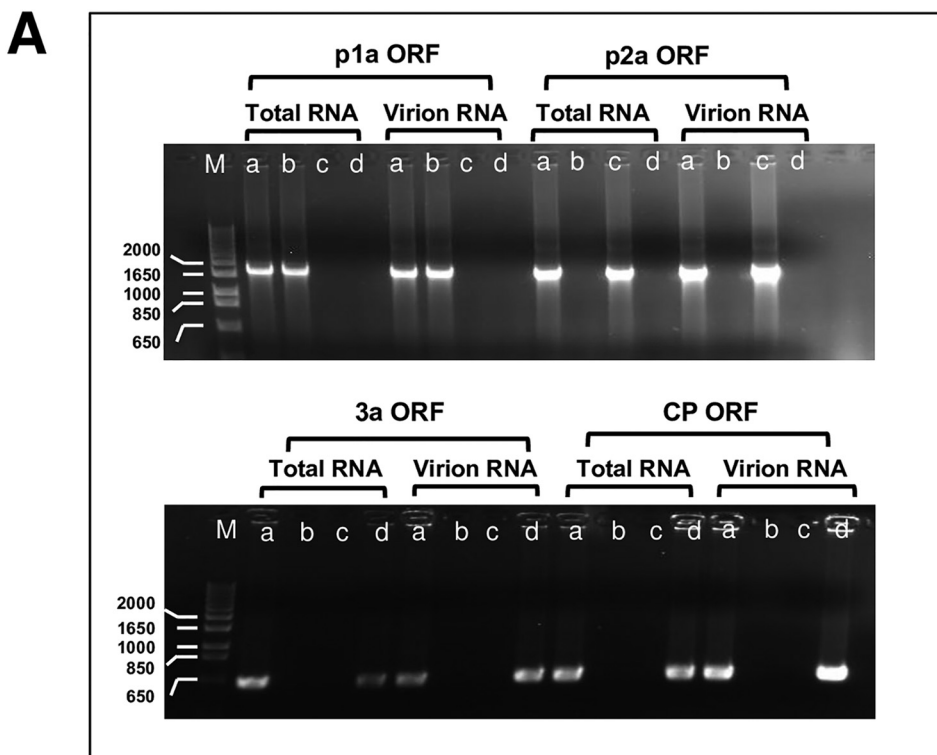
FIG 4 Physical characterization of B1ᵛ, B2ᵛ, and B3+4ᵛ. (A) Negative-stain electron micrographs of density gradient-purified virions of either wt BMV from mechanically inoculated *N. benthamiana* or barley plants or autonomously assembled virions of B1ᵛ, B2ᵛ, B3+4ᵛ, and BCPᵛ via agroinfiltration. Graphic representations shown below each image show a histogram of the virion sizes obtained by measuring at least 100 virions/sample. (B) Virion electrophoresis. Density gradient-purified virions of CCMV (lane 1), BMV (lane 2), B1ᵛ (lane 3), B2ᵛ (lane 4), and B3+4ᵛ (lane 5) were subjected to agarose gel analysis as described in Materials and Methods. Gel shown at the top was stained with ethidium bromide to detect RNA and then restained with Coomassie blue to detect protein (bottom panel). BMV and CCMV virions migrating toward negative and positive, respectively, are indicated.

symptoms characteristic of wt BMV (11) were observed only when the inoculum contained a mixture of all three virion types (i.e., B1ᵛ+B2ᵛ+B3+4ᵛ) but not with either individual (i.e., B1ᵛ, B2ᵛ, or B3+4ᵛ) or pairwise combinations (i.e., B1ᵛ+B2ᵛ, B1ᵛ+B3+4ᵛ, or B2ᵛ+B3+4ᵛ). Taken together, these results confirm that B1ᵛ, B2ᵛ, and B3+4ᵛ are highly pure and completely free from their counterparts.

Virion stability of B1ᵛ, B2ᵛ, and B3+4ᵛ. To test the relative thermal stability of B1ᵛ, B2ᵛ, and B3+4ᵛ, a differential scanning fluorimetry (DSF) assay was performed as described in Materials and Methods. The hydrophobic dye used in this assay increases the intensity of the fluorescence following its binding to the accessible hydrophobic regions of the viral CP during thermal denaturation (23). Results of the DSF analysis of the temperature-dependent melting of virions of B1ᵛ, B2ᵛ, and B3+4ᵛ and control samples (wt BMV and lysozyme) under three buffer and pH conditions are summarized in Fig. 6. Thermal denaturation in water showed a clear difference between virions of B1ᵛ and B2ᵛ and those of B3+4ᵛ (Fig. 6A), For example, virions of B1ᵛ and B2ᵛ displayed melting of thermally unstable populations at ~50°C and ~70°C (Fig. 6A, left and middle). By contrast, virions of B3+4ᵛ melted only at ~70°C (Fig. 6A, left and middle). Analysis of the three virion types by DSF in virus suspension buffer (pH 4.5) and phosphate buffer (pH 7.2) revealed identical thermal stability profiles, the least stable

FIG 5 Genome content and infectivity of B1^V, B2^V, and B3+4^V. (A) RT-PCR analysis. Agarose gel analysis of RT-PCR products amplified from total RNA and virion RNA of wt BMV (a), B1^V (b), B2^V (c), and B3+4^V (d) using a set of primers designed to specifically amplify the regions encompassing either p1a ORF, p2a ORF, 3a ORF, or CP ORF as described in Materials and Methods. M, marker lane. (B) Infectivity assays. *C. quinoa* leaves were mechanically inoculated with either wt BMV or agrotransformants of B1^V, B2^V, or B3+4^V in the indicated combinations. Presence (+) or absence (−) of local and systemic infection characteristic of BMV was monitored and recorded over a period of 2 weeks.
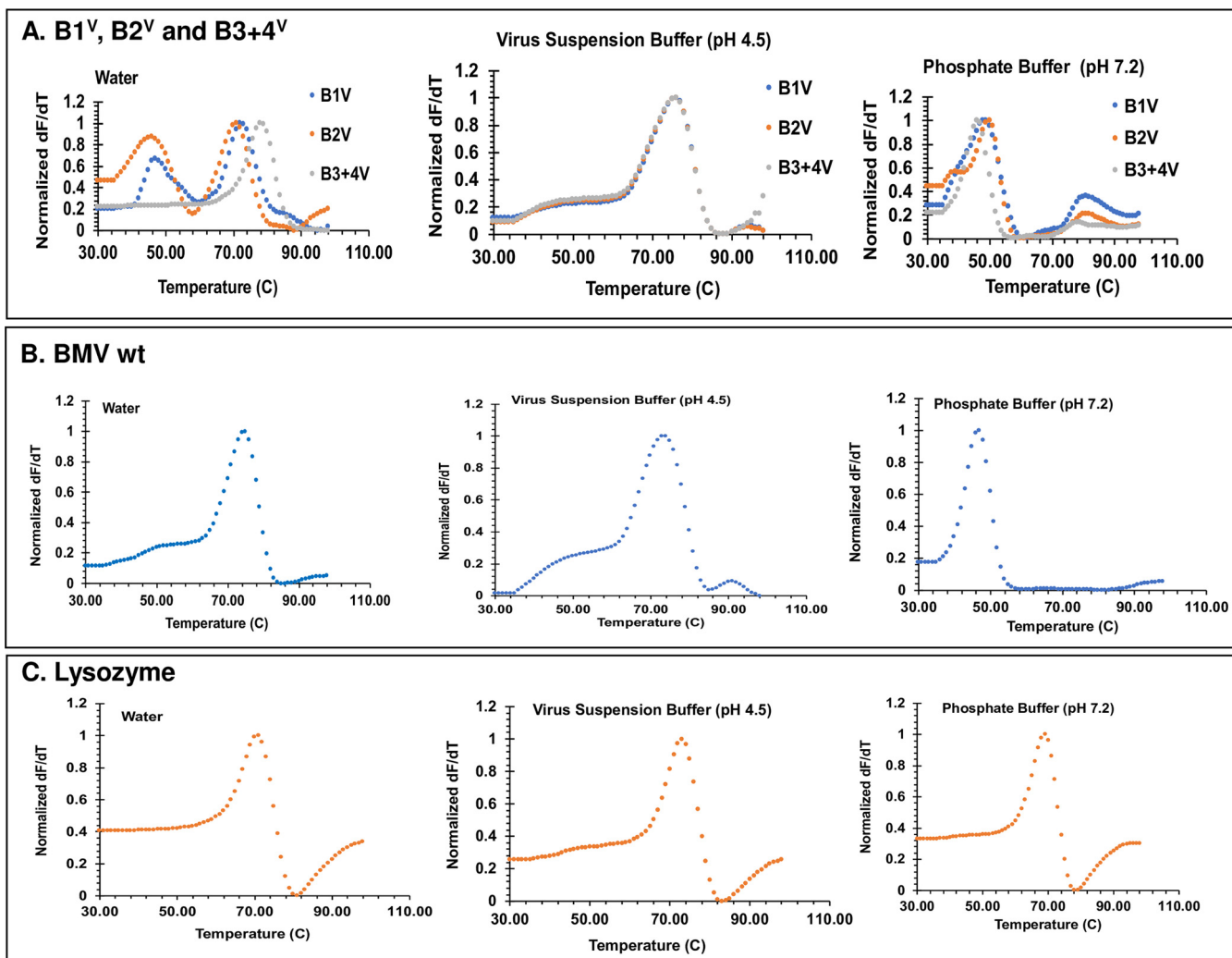
FIG 6 Stability analysis of the three BMV virion types using differential scanning fluorimetry (DSF). DSF measurements of derivative of fluorescence intensity as a function of temperature for each virion type normalized so that the maximum of the derivative is set to 1 (y axis) during heating of B1^V, B2^V, and B3+4^V (A), wt BMV (control) (B), and lysozyme (control) (C) at various temperatures (x axis) under indicated conditions. Although virions of wt BMV and B1^V, B2^V, and B3+4^V displayed identical temperature dependence (~70°C) for melting in all three solutions, a portion of virions of B1V and B2V melted at lower temperatures (see "Virion stability of B1V, B2V, and B3+4V" for details). Lysozyme used as a positive control showed identical melting characteristics (~60°C) under all three solution conditions.

being in phosphate buffer (Fig. 6A, right). Interestingly, a different scenario was observed for wt BMV (Fig. 6B). The majority of the wt BMV virions remained thermally stable in water and virus suspension buffer and displayed a small shoulder peak at ~50°C (Fig. 6B, left and middle). Since wt BMV represents a disproportionate mixture of three virion types (Fig. 1C), it is likely that the shoulder peak represents virions of B1^V and B2^V, as shown in Fig. 6A. As expected, the thermal stability of lysozyme remained indistinguishable under all three buffer conditions (Fig. 6C).

Analysis of the capsid dynamics of B1^V, B2^V, and B3+4^V by MALDI-TOF. One of the promising approaches in distinguishing crystallographically identical viral capsids involves the use of limited proteolysis followed by the identification of the cleavage products of the capsid subunits by mass spectrometry (24). Proteolytic cleavage sites present on the exterior of the capsid will be most accessible to the enzyme and therefore will be among the first digestion fragments observed. Consequently, MALDI-TOF analysis of proteolytic cleavage products would contribute to understanding the dynamic domains within the capsid structure (24, 25).

First, the relative capsid dynamics were investigated by trypsin digestion performed at various time points to verify whether B1^V, B2^V, and B3+4^V virion types display any
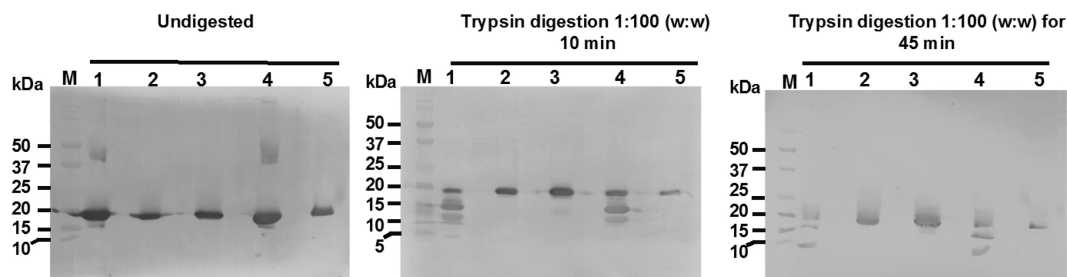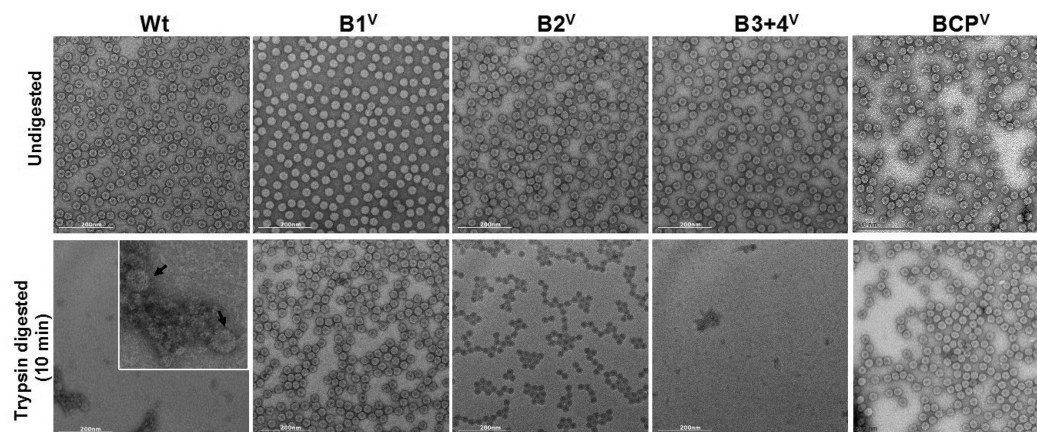
(A) Western blot analysis

(B) EM analysis

FIG 7 Proteolysis of B1^V, B2^V, and B3+4^V monitored by Western blotting and negative-stain EM analysis. (A) Western blot for wt BMV (lane 1), B1^V (lane 2), B2^V (lane 3), B3+4^V (lane 4), and BCP^V (lane 5). Prior to Western blot analysis, each virion preparation was either undigested (left) or digested with trypsin for 10 min (middle) or 45 min (right). (B) Negative-stain electron micrographs show the integrity of the undigested and trypsin-digested virion preparations of the indicated samples. (Inset) Arrows indicate intact virions of trypsin-resistant B1^V and/or B2^V.

discernible effect on the rate of digestion (see Materials and Methods). Parallel diges-tions were performed with virions of wt BMV (mixture of all three virion types) and BCP^V (assembled in the absence of the viral replicase and packaging cellular RNA) as controls. Trypsin cleaves peptides on the C-terminal side of lysine and arginine residues (X-K/-X and X-R/-X); furthermore, if a proline residue is on the carboxyl side of the cleavage site, the cleavage will not occur. Therefore, the BMV CP linear sequence that is 189-aa long has 22 potential trypsin cleavage sites (26). Following trypsin digestion, each virion type preparation was divided in half. One half was subjected to Western blot analysis using an anti-CP antibody to identify the cleavage peptides, while the second half was subjected to EM analysis to verify the integrity of virions. Results are summarized in Fig. 7A and B. Undigested CP of virions of control samples (Fig. 7A, left, lanes 1 and 5) as well as all three individual virion types (B1^V, B2^V, and B3+4^V) (Fig. 7A, left, lanes 2 to 4) migrated as a single intact band with the expected molecular weight (~20 kDa). Analysis of the trypsin cleavage products for each virus sample revealed interesting profiles. For virions of wt and type 3 (B3+4^V), trypsin digested >50% of the CP, resulting in three faster-migrating peptide fragments in addition to a single intact protein band (Fig. 7A, middle, lanes 1 and 4). Based on the mass spectrometry data, these fragments correspond to residues 15 to 189, 27 to 189, and 43 to 189 (data not shown). By contrast, digestion of virion types 1 and 2 and BCP with trypsin failed to yield any detectable peptide fragments on the Western blot (Fig. 7A, middle, lanes 2, 3, and 5) and are indistinguishable from those of undigested samples (Fig. 7A, left, lanes 2, 3, and 5). These profiles did not change even after the digestion time to trypsin was extended (10 and 45 min) (Fig. 7A, right; Table 1). Electron microscopic analysis of

TABLE 1 Kinetics of trypsin cleavage sites located on B1^V, B2^V, and B3+4^V

Residues	Sequence	m/z	Time to cleavage							
			10 min–18 h		B3+4^V					
			B1^V	B2^V	10 min	20 min	30 min	45 min	3 h	18 h
2–8	STSGTGK	679.3257	+	+	−	−	−	+	+	−
20–26	RNRWTAR	959.5282	−	−	+	+	+	+	−	−
21–26	NRWTAR	803.4271	−	−	+	+	+	+	+	+
27–41	VQPVIVEPLAAGQGK	1,505.8686	−	−	+	+	+	+	−	−
27–64	VQPVIVEPLAAGQGKAIKAIAGYSISKWEASS DAITAK	3,868.1219	−	−	+	+	+	+	−	−
42–64	AIKAIAGYSISKWEASSDAITAK	2,381.2711	−	−	+	+	−	−	−	−
45–64	AIAGYSISKWEASSDAITAK	2,069.055	−	−	−	−	−	+	−	−
54–64	WEASSDAITAK	1,178.5688	−	−	−	+	−	−	−	−
65–81	ATNAMSITLPHELSSEK	1,828.9109	−	−	−	+	+	+	−	+
65–83	ATNAMSITLPHELSSEKNK	2,071.0488	−	−	+	+	−	−	−	−
65–86	ATNAMSITLPHELSSEKNKELK	2,441.2705	−	−	+	+	−	+	−	−
65–89	ATNAMSITLPHELSSEKNKELKVGR	2,753.4614	−	−	+	+	+	−	−	−
84–103	ELKVGRVLLWLGLLPSVAGR	2,176.3329	−	−	+	−	−	−	−	−
84–105	ELKVGRVLLWLGLLPSVAGRIK	2,417.5119	−	−	−	−	−	−	+	−
87–103	VGRVLLWLGLLPSVAGR	1,806.1112	−	−	+	−	−	−	−	−
90–103	VLLWLGLLPSVAGR	1,493.9202	−	−	+	+	−	−	+	+
104–111	IKACVAEK	861.4863	−	−	−	+	−	−	−	−
106–111	ACVAEK	620.3072	−	−	−	−	−	−	+	−
112–130	QAQAEAAFQVALAVADSSK	1,904.9712	−	−	+	+	+	−	+	−
112–142	QAQAEAAFQVALAVADSSKEVVAAMYTDAFR	3,258.61	−	−	+	+	+	+	−	−
131–142	EVVAAMYTDAFR	1,372.6566	−	−	+	+	+	+	+	+
166–189	AVVVHLEVEHVRPTFDDFFTPVYR	2,872.4781	−	−	+	+	+	+	+	+

trypsin-digested virion preparations (Fig. 7B) confirmed the Western blot data, showing that virions of type 1 and 2 as well as BCP are structurally intact, while those of wt and type 3 are unstable and degraded rapidly.

Next, MALDI-TOF was used to identify the cleavage products present in the trypsin-digested virion samples. The deconvoluted mass spectrum obtained from the total ion chromatogram (TIC) of the undigested virions of wt, B1^V, B2^V, B3+4^V, and BCP^V indicate that all the virions are assembled from a single protein of 20,296 Da, which underlines their purity. A representative example of the deconvoluted mass spectrum of undigested virions is shown in Fig. 8A.

Analysis of the released peptides after 10, 20, 30, and 45 min clearly distinguished virions of B1^V and B2^V from those of B3+4^V: virions of B1^V and B2^V are grouped into class I and those of B3+4^V into class II. Although early time points of the reaction are indicative of the very first sites of protease cleavage (25), the trypsin digestion pattern for B1^V and B2^V is similar and domain specific irrespective of time of exposure, either early (10 and 20 min) or late (30 min, 45 min, and 3 h) (Table 1). MALDI-TOF mass mapping identified a prominent but low-abundance fragment corresponding to the N-terminal 2 to 8 aa (Fig. 8B and D). The authenticity of the 2 to 8 aa fragment was confirmed when the mass spectrum between 670 to 690 m/z was analyzed (Fig. 8C and E). Trypsin digestion did not release any peptide beyond 2 to 8 aa (Fig. 8F and G). Extending the trypsin digestion time to 3 h and 18 h did not change the cleavage pattern (Table 1). Although highly basic, the N-proximal region is predicted to be mobile/disordered and internalized following its interaction with RNA (9). Taken together, these data suggest that in B1^V and B2^V, only the N-terminal ARM region, encompassing aa 2 to 8, which is crystallographically defined as being internal to BMV, is made accessible to protease digestion.

The scenario and the rate at which virions of B3+4^V are digested by trypsin are observed to be qualitatively distinct from those of B1^V and B2^V. For example, Western blot analysis revealed that for virions of B3+4^V, the intact protein present in trypsin-digested sample was less than 50% compared to that of either untreated B3+4^V or trypsin-treated B1^V and B2^V samples (Fig. 7A). At every time point examined, including the early time points (e.g., 10 and 20 min), virions of B3+4^V were highly susceptible to
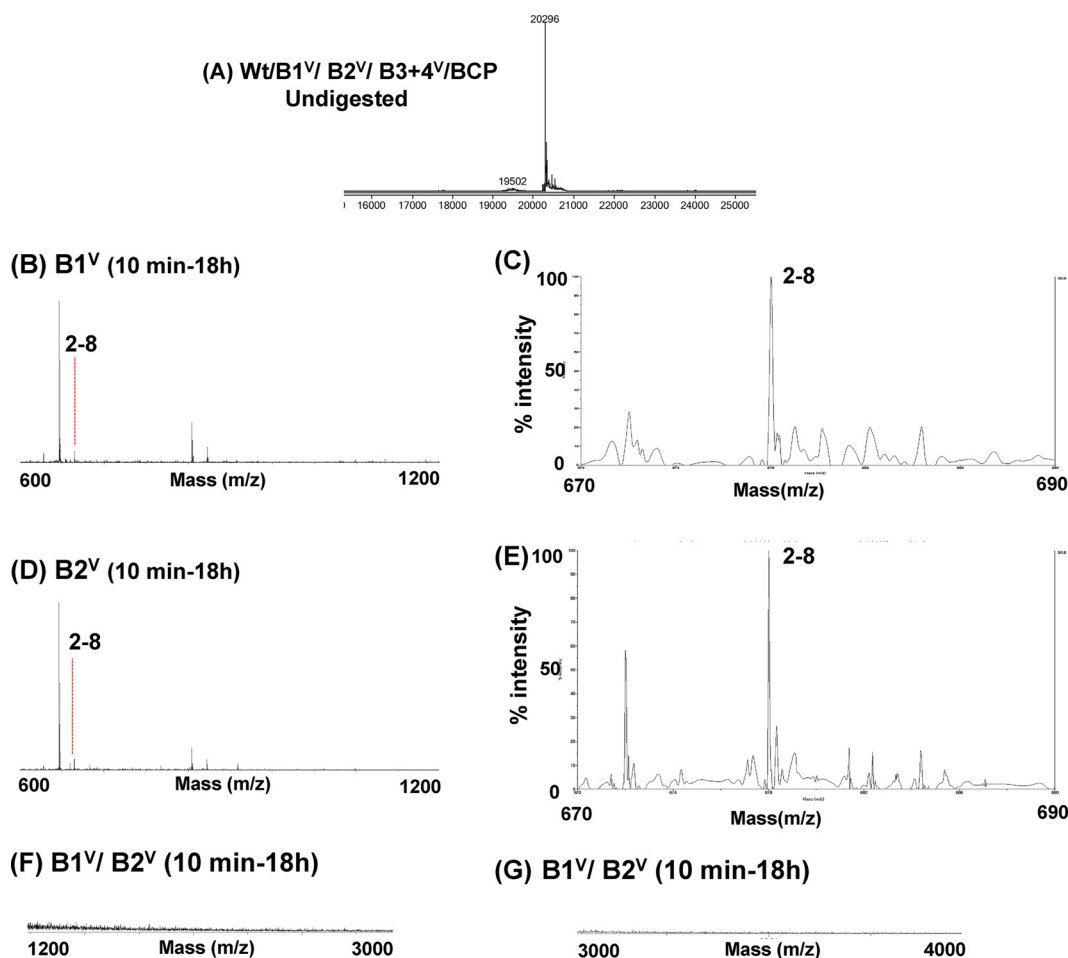
FIG 8 MALDI-TOF analysis of undigested and trypsin-digested virions. (A) Mass spectrometry of undigested virions of wt, B1^V, B2^V, B3+4^V, and BCP^V yielded a single peak with a value of 20,296 Da. MALDI-TOF analysis of peptides released from B1^V (B, F and G) and B2^V (D, F and G) following digestion with trypsin at the indicated time points. (C and E) Authenticity (intensity nearing 100%) of a peptide corresponding to 2 to 8 aa of the N-ARM in B1^V and B2^V when the mass spectrum between 670 to 690 m/z was analyzed. Peaks are labeled with corresponding polypeptide fragments of indicated amino acids residues. Table 1 summarizes masses and identifies the corresponding amino acid residues.

trypsin, releasing multiple peptides. Identification of the released peptides by mass mapping revealed that the accessible trypsin cleavage sites (e.g., K^{65}, R^{103}, K^{111}, and K^{165}) (Fig. 9; Table 1) were consistent with the reported surface structure of the BMV virions (9) (see Discussion). This explains why EM shows the trypsin-treated virions of B3+4^V to be visibly degraded (Fig. 7B). These observations suggest that virions of B3+4^V are either dynamically distinct from those of B1^V and B2^V and/or that the two virion types are conformationally different in the exterior arrangement of the CP amino acid residues. Although peptides representing N-terminal regions (21 to 26 aa) were detected at the earliest time point (e.g., 10 min) (Fig. 9), their accessibility to protease coincided with other cleavage sites as well (Fig. 9; Table 1). Therefore, it is likely that these N-terminal peptides on virions of B3+4^V may not be the first sites of protease cleavage, since multiple simultaneous cleavages at other sites expose the otherwise internalized N-terminal region to proteolysis (see Discussion). A similar explanation can account for the detection of peptides encompassing the N-ARM region of 2 to 8 aa after extended periods of digestion (e.g., 45 min in Fig. 9; Table 1). The rationale and biological significance for the different surface configurations of the individual virions of the tripartite BMV are discussed below.

Figures 7A and 10 summarize the Western blot analysis of trypsin digestion products and their MALDI-TOF analysis, respectively, for the virions of the wt BMV and BCP^V used
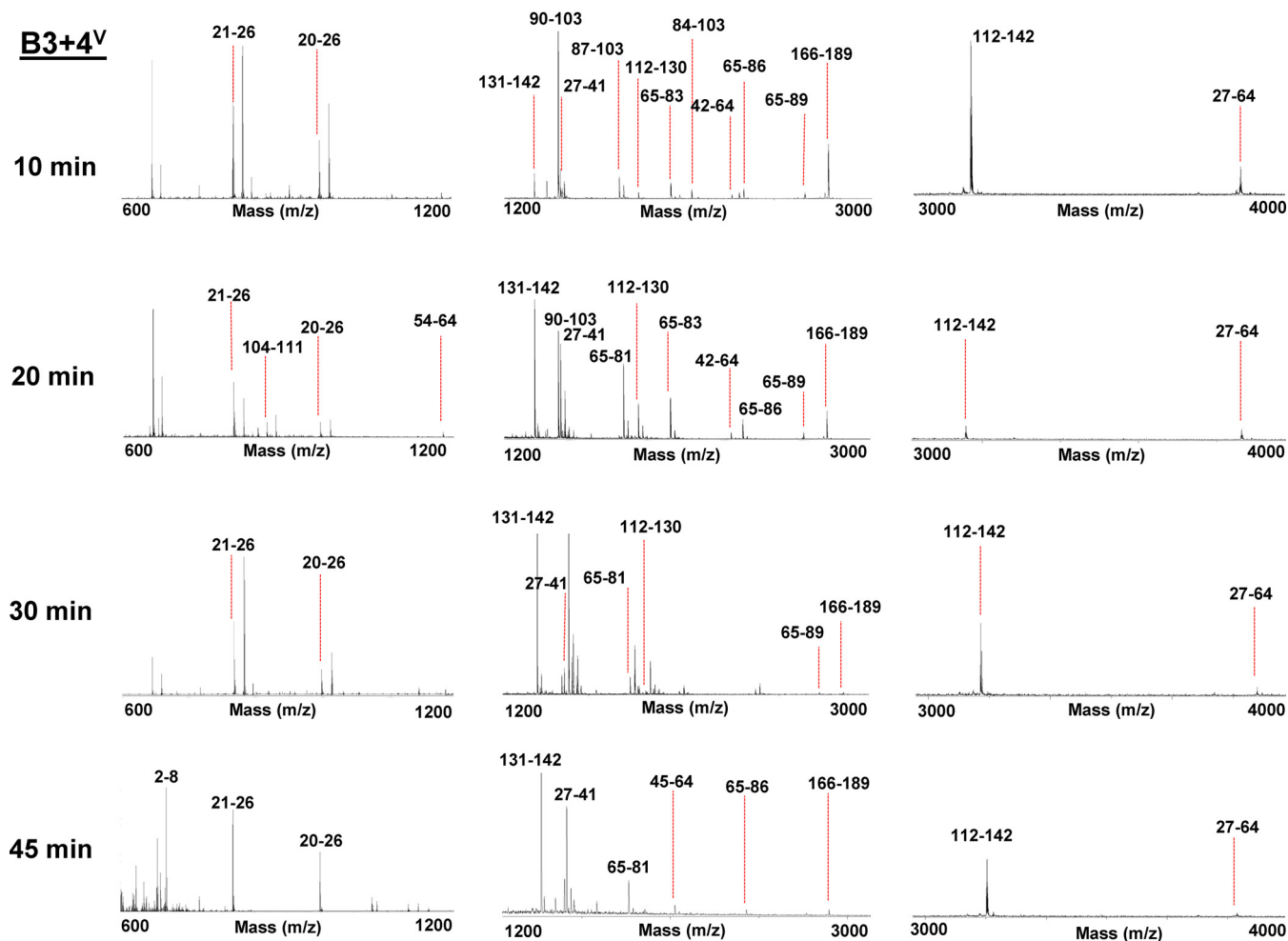
FIG 9 MALDI-TOF analysis of peptides released from B3+4^V following trypsin digestion at the indicated time points. Peaks are labeled with corresponding polypeptide fragments of indicated amino acids residues. Table 1 summarizes masses and identifies the corresponding amino acid residues.

as controls. The digestion profiles of wt BMV are identical to those of B3+4^V (Fig. 7, 9, and 10). By contrast, unexpected trypsin cleavage profiles were obtained for BCP^V (Fig. 10). Although BCP^V virions are distinct in size and RNA packaging traits compared to those of wt BMV (15), remarkably, their sensitivity to trypsin digestion and subsequent MALDI-TOF profiles are shared with those of B1^V and B2^V (Fig. 10; Table 1). We speculate that some of the unassigned peaks observed in MALDI-TOF analysis (Fig. 8 and 10) may be the result of trypsin self-cleavage (http://prospector.ucsf.edu/prospector/mshome .htm). For brevity, Fig. 11 summarizes the location of the trypsin cleavage sites identified to be located on B1^V, B2^V, and B3+4^V by MALDI-TOF.

DISCUSSION

Following entry to a susceptible host cell, viruses face a daunting challenge of not only surviving in the harsh cellular environment, but they must also release their genome to perform various functions in establishing an infection. A series of biochemical and biophysical studies with a range of viruses has revealed that viral capsids undergo controlled conformational transitions to alter the surface structures compatible with disassembly and release of the genome when required (1, 3). The primary focus of our present study is to investigate whether physically indistinguishable virions of BMV—each with a different RNA content—can be distinguished in solution, as demonstrated for other RNA viruses such as members of the families *Nodaviridae* (3, 23) and *Picornaviridae* (25). Using agroinfiltration, we were successful in assembling, for the
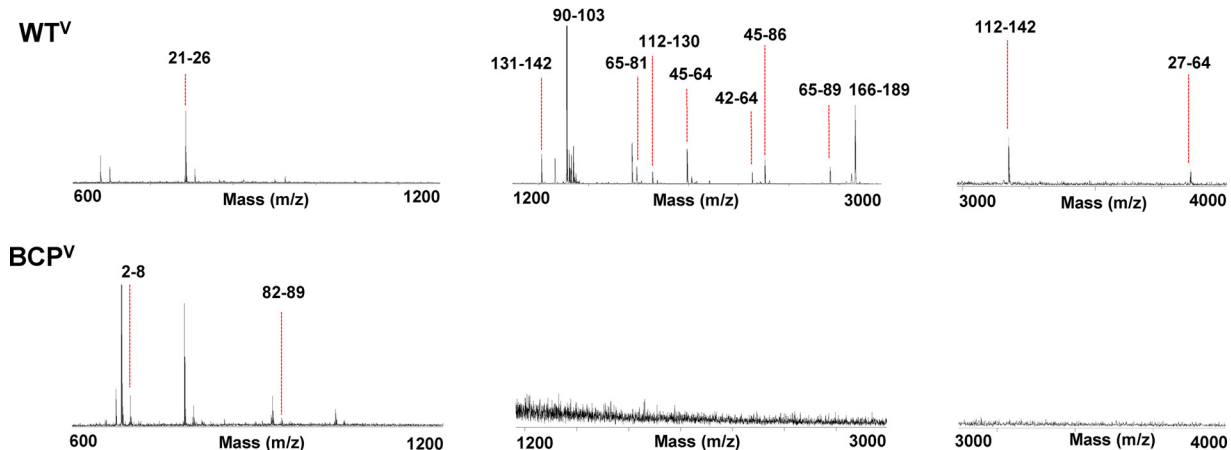
FIG 10 MALDI-TOF analysis of peptides released from virions of wt BMV and BCP[V] following trypsin digestion at 10 min. Peaks are labeled with corresponding polypeptide fragments of indicated amino acids residues. Table 1 summarizes masses and identifies the corresponding amino acid residues.

first time, the three virion types of BMV, B1[V], B2[V], and B3+4[V] separately *in planta*, virions which are otherwise impossible to separate in pure forms (8). A series of biochemical (e.g., RT-PCR) (Fig. 5A) and biological assays (Fig. 5B) established the purity of each virion type. Although the three virion types are physically and morphologically indistinguishable (Fig. 4A), application of thermal denaturation analysis and limited proteolysis with trypsin followed by MALDI-TOF distinguishes between two dynamical classes of the three virion types: B1[V] and B2[V] are grouped into class I and B3+4[V] as class II. Below, we discuss the biological significance of this distinction.
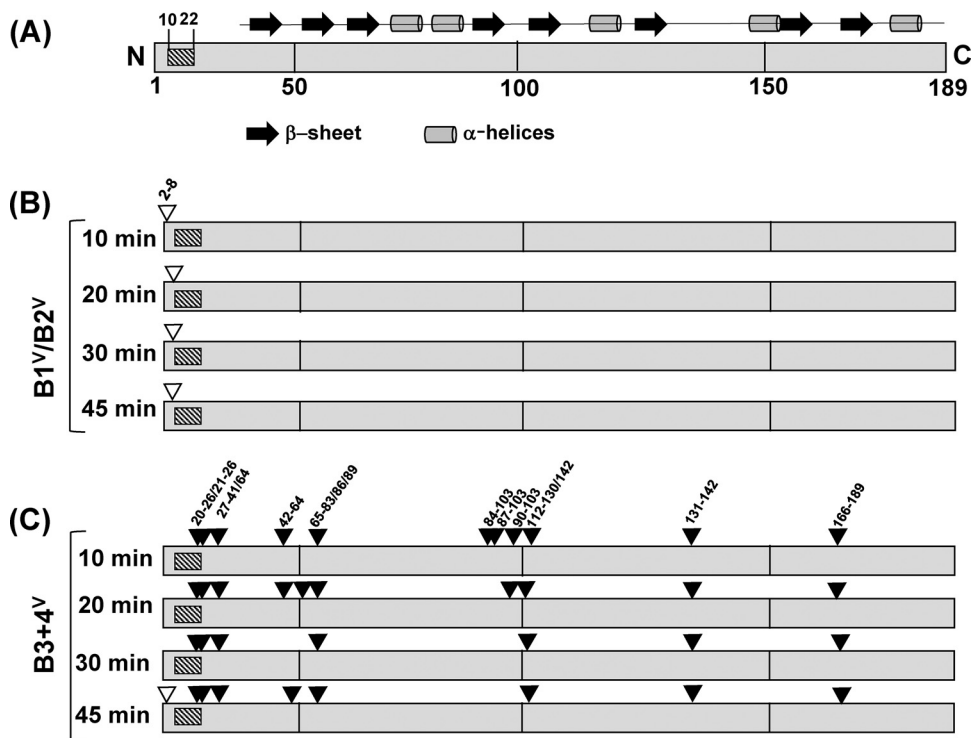

FIG 11 Summary of proteolytic cleavage sites mapped to the virions of B1[V], B2[V], and B3+4[V]. (A) Schematic representation of linear representation of the 189 aa of the BMV CP subunit. Location of the arginine-rich motif (ARM) at aa 10 to 22 in the N-proximal region is indicated as a stippled box. (B) Empty arrowheads represent the trypsin-accessible sites located in the N-ARM regions of B1[V] and B2[V] (B) and B3+4[V] (C), whereas filled arrowheads indicate the trypsin-accessible sites present at other locations on the CP.

Virions of B1^V and B2^V are dynamically distinct from those of B3+4^V. Prior to this study, separation of the three types of virions into individual components by multiple rounds of CsCl$_2$ buoyant density centrifugation (13, 14) had resulted only in the enrichment of a given virion type rather than freeing it completely from the other two components. By contrast, the feasibility of assembling pure B1^V, B2^V, and B3+4^V virion types has been demonstrated by the strategy shown in Fig. 3C to E).

Although EM analysis (Fig. 4A) and electrophoretic mobility profiles (Fig. 4B) suggest that virions of B1^V, B2^V, and B3+4^V are physically indistinguishable and homogeneous, limited proteolysis followed by MALDI-TOF analysis proved otherwise. Based on the BMV structure model (9), the four accessible trypsin cleavage sites (K^{65}, R^{103}, K^{111}, and K^{165}) located on the surfaces of the A, B, and C subunits of BMV CP are shown in Fig. 12. Arginine and lysine residues located in the highly basic N-proximal region (e.g., K^8, R^{11}, and R^{14}) are least exposed (Fig. 12) and predicted to internalize by interacting with the packaged RNA (9). Consequently, these are not expected to be accessible for trypsin cleavage.

Identification of the cleavage products of B1^V, B2^V, and B3+4^V at various time points by mass mapping suggested the following: (i) for B1^V and B2^V, the N-proximal ARM region encompassing aa 2 to 8 is transiently exposed on the capsid surface. Since N-terminal residues 1 to 27 are not ordered in the crystal structure (9), their cleavage did not affect the structural integrity of the virions (Fig. 7B). (ii) For B3+4^V, amino acids K^{65}, R^{103}, K^{111}, and K^{165} are located on the surface of the capsid and hence are readily accessible for cleavage. In BMV, the stability of noncovalent dimers, the building blocks of icosahedral viruses (27, 28), is controlled by the interaction between the invading C-terminal arm and the N-terminal clamp of the adjacent CP subunits, and any mutations engineered in the C terminus disrupt virion assembly (28, 29). Thus, cleavage at K^{165} alone is sufficient to disrupt the capsid structure. This explains why B3+4^V appears visibly degraded in EM (Fig. 7B). Detection of peptides encompassing the N-proximal 21 to 26 and 20 to 26 aa region at an early time point (10 min) suggests their externalization in B3+4^V (Fig. 9). Alternatively, it is likely that the extensive cleavage of the capsid as early as 10 min by trypsin (Fig. 9) results in degradation of the capsid structure (Fig. 7B), which leads to externalization of the N terminus and its subsequent proteolysis.

MALDI-TOF analysis profiles of wt BMV virions are indistinguishable from those of B3+4^V (Fig. 11). This is not surprising, since purified virion preparation of wt BMV is a mixture of all three virion types, with B3+4^V constituting ~60% of the total (Fig. 1C). However, virions of BCP, characterized by the distinct virion phenotype packaging cellular RNA (15), remained highly resistant to trypsin (Fig. 7A and B) and positioned the N-proximal 2 to 8 aa peptides externally to the capsid (Fig. 10). Although the reasons for the unexpected dynamics are currently unclear, it is possible that the type of RNA packaged influences the observed conformational dynamics.

A couple of previous studies have attempted to analyze the dynamics of bromoviral capsids without using pure virion type as reported in this study. For example, when the dynamics of wt CCMV and a salt-stable variant of CCMV (SS-CCMV) (25) were compared, it was observed that wt CCMV particles are more sensitive to trypsin than SS-CCMV. However, the pattern of released peptides is similar for both forms of CCMV, and the reported cleavage sites were localized to the N terminus of the CP (25). In contrast to CCMV, Vaughan et al. (14) attempted to segregate each virion type of BMV using CsCl$_2$ centrifugation, even though BMV has been shown to be unstable in CsCl$_2$ due to its "salt-labile" nature (30–32). However, they were only successful in getting the fractions enriched in a given virion type (i.e., not free from remaining counterparts). The results obtained using contaminated virion fractions in conjunction with a different protease (broadly specific proteinase K), coupled with the fact that B3+4^V constitutes ~60% of the total virion population (Fig. 1C) and that B1^V and B2^V are dynamically distinct from those of B3+4^V (shown in this study), make the comparison of our results to those of Vaughan et al. (14) problematic.
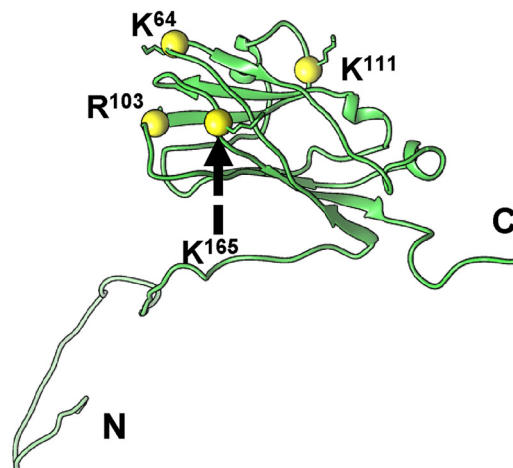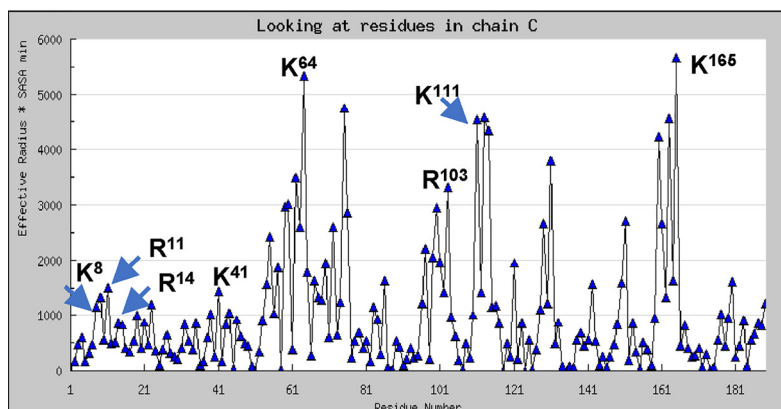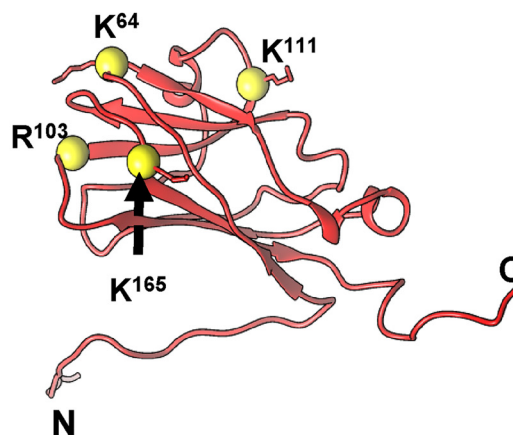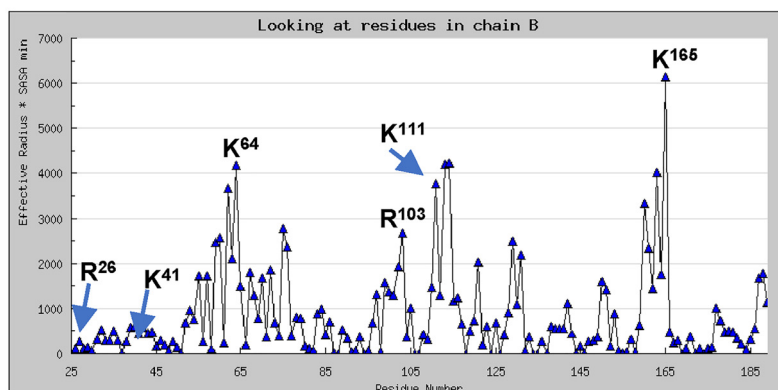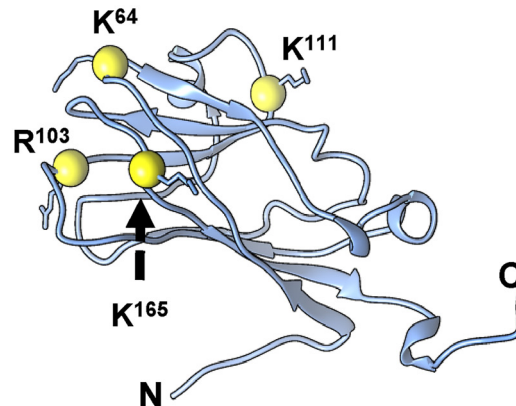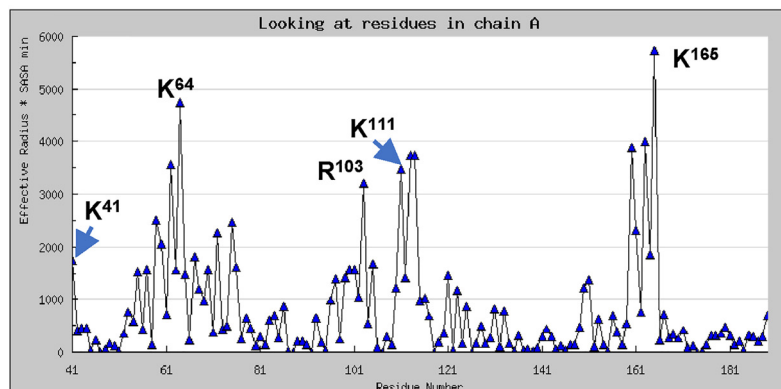
FIG 12 Location of the amino acid sites accessible for trypsin digestion on the A, B, and C subunits of the BMV CP (http://viperdb.scripps.edu/). Location of trypsin sites on A, B, and C subunits of BMV CP.

Biological significance. Based on our initial results comparing the stability (Fig. 6) and proteolysis profiles (Fig. 8 and 10) for B1^V and B2^V on the one hand and B3+4^V on the other, we hypothesize that the stability and conformational fluctuations displayed by B1^V and B2^V versus that of B3+4^V are linked to a specific role during the establishment of infection in a given host. For example, in B1^V and B2^V, the N-proximal 2 to 8 aa region is transiently externalized, allowing the virions to retain their structural integrity
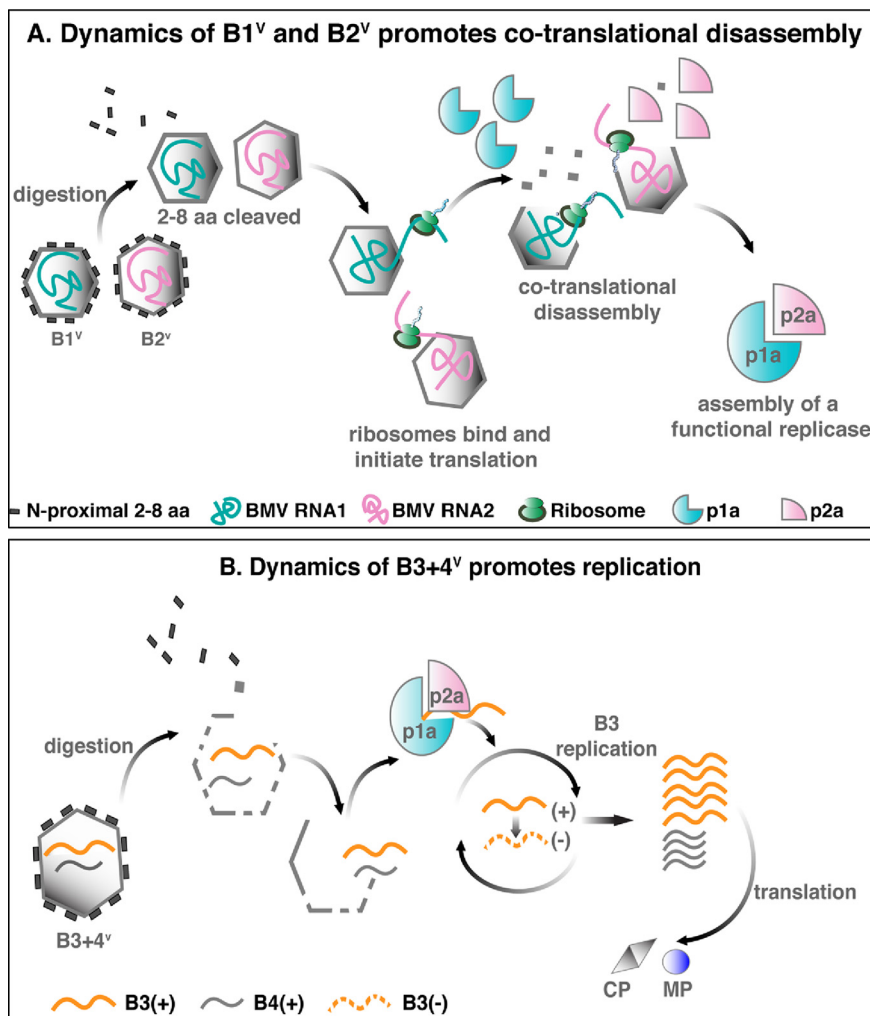
FIG 13 A schematic model showing a role for the externalization (in B1^V and B2^V) and internalization (in B3+4^V) of the CP-N-proximal region in translation and replication, respectively. BMV replication requires both p1a and p2a (33) and occurs in ER-derived vesicles or spherules whose formation is mediated by p1a (34, 35). Therefore, following virus entry, B1 and B2 RNAs must be available to the translational machinery, and this is facilitated by fluctuation of the N terminus outside the capsid, as shown for B1 and B2 virions (Fig. 11A), which carries with it the 5′ RNA end needed for ribosomal binding followed by cotranslational disassembly. In contrast, the B3+4^V (Fig. 11B) virions make their RNA available to replication by the replicase complex, resulting in the synthesis of sgRNA4 from replication-derived minus-strand B3 progeny (7) for translation of the CP that stimulates plus-sense RNA synthesis over that of minus-sense RNA (36). See "Biological significance" for details.

following trypsin digestion (Fig. 7B), suggesting the scenario shown in Fig. 13A. It is well established that the primary phase in the infection cycle of BMV (and other RNA viruses as well) is the production of replicase proteins. BMV replication requires both p1a and p2a (33) and occurs in ER-derived vesicles or spherules, and their induction is mediated by p1a (34, 35). Therefore, following viral entry, the instability under neutral pH conditions and the observed capsid dynamics allow ribosomes to bind B1 and B2 RNA and initiate translation of p1a and p2a, respectively (Fig. 13A). Instability of the virions in conjunction with translation of B1 and B2 RNA leads to cotranslational disassembly of B1^V and B2^V (Fig. 13A).

A contrasting scenario is proposed for the virions of B3+4^V (Fig. 13B). Unlike the genomic RNAs B1 and B2, replication is favored over translation for the genomic RNA B3 for the following reason. In BMV, CP plays a multifunctional role, including the stimulation of plus-strand synthesis over that of minus strands (36) by interacting with replicase protein p2a (18, 37). Thus, in order to synthesize CP, RNA3 must undergo

replication to generate CP mRNA, i.e., sgB4. As in B1^V and B2^V, the N terminus of the CP in B3+4^V virions is not exclusively sensitive to trypsin digestion (Fig. 9 and 11C), suggesting that the N-ARM region is internal and not exposed outside the capsid, resulting in B3 RNA being unavailable for translation initiation. Virions of B3+4^V are highly sensitive to trypsin (Fig. 7B), resulting in complete release of their RNA. Consequently, the internalization and the interaction between the N-ARM and B3 inhibit translation and favor replication.

In conclusion, results of this study represent a starting point toward understanding the differences among the otherwise structurally indistinguishable three virion types of BMV. Our results obtained analyzing the virion stability and capsid dynamics place BMV in a new perspective and shed light in understanding the overall biology of the virus. The strategy used to assemble independent virions of BMV (Fig. 3) is applicable to other RNA viruses and specifically to multicomponent viruses, such as cucumber mosaic virus, that exhibit particle homogeneity similar to that of BMV. Finally, the independently assembled virion types of BMV are ideal candidates for determining the structure of each virion type and the application of single-particle tomography (38, 39) to complete the map of the conformational heterogeneity in these virion types.

MATERIALS AND METHODS

Agroplasmids used in this study. Construction and characteristic properties of agroplasmids pB1, pB2, and pB3 (Fig. 2A), engineered to express biologically active full-length genomic RNAs of BMV following agroinfiltration into plants, were described previously (15). Likewise, agroplasmids p1a, p2a, and pCP (Fig. 2B) were engineered to transiently express replicase protein 1a (p1a), replicase protein 2a (p2a), and CP, respectively, as described previously (15, 40).

Virion purification, negative-stain electron microscopy, virion RNA electrophoresis, and Western blot analysis. The procedure used to purify BMV virions from agroinfiltrated leaves 4 to 6 days postinfiltration (dpi) followed by sucrose density gradient centrifugation was as described by Rao et al. (41). For negative-stain EM analysis, gradient-purified virions were spread on glow-discharged grids followed by negative staining with 2% uranyl acetate prior to examination with a Tecnai F20 transmission electron microscope operated at 200 KeV (The Core Microscopy Facility, The Scripps Research Institute, La Jolla, CA). EM images were collected using Leginon program. Virions of BCP were imaged at UC-Riverside (UCR) using a Tecnai 12 operated at 120 KeV, and images were recoded digitally. For electrophoretic mobility analysis, purified virions were loaded in a 1% agarose gel, prepared, and electrophoresed in BMV suspension buffer at 7 V/cm for 2 to 2.5 h at 4°C. For RNA analysis, virion RNA was electrophoresed in 1.2% agarose gels under denaturing conditions as described previously (15). Following ethidium bromide staining, quantitation of each RNA was performed using Image J software (42). Western blot analysis of undigested and trypsin-digested virion samples using anti-CP antibodies was performed as described previously (15).

Differential scanning fluorimetry. DSF was performed essentially as described previously (23). Desired virus and control (lysozyme) samples were resuspended either in Nanopure sterile water (pH 7.1), in virus suspension buffer (50 mM sodium acetate, 8 mM magnesium acetate, pH 4.5), or in 100 mM phosphate buffer (pH 7.2). The experiment was performed three times independently using three replicates for each sample. DSF data were analyzed and plotted as described by Rayaprolu et al. (23).

MALDI-TOF. For MALDI-TOF analysis, a desired purified virion preparation was diluted to 1 mg/ml in 25 mM Tris-HCl, 1 mM EDTA buffer. A 30-μl sample (i.e., 30 μg of the virus) was digested with a 1:100 (wt/wt) ratio of trypsin (Pierce Trypsin protease, mass spectrometry grade; Thermo Fisher Scientific) to virus for various time points at 25°C (19, 24). Twenty microliters of water was added to 10 μl of the digested sample, and approximately 0.5 μl of each digested or undigested (control) sample was analyzed on an AB Sciex TOF/TOF 5800 MALDI MS with α-cyano-4-hydroxycinnamic acid matrix. The instrument was calibrated with standards, and the test samples were analyzed with external calibration. The accuracy is approximately ±0.05 Da. The MALDI-TOF data were analyzed with AB Sciex Data Explorer, and baseline was corrected with peak width of 32, flexibility of 0.5, and degree of 0.1. For noise removal, the standard deviation was set at 2. To determine the peak detection criteria, percent centroid was taken as 50, signal/noise (S/N) threshold was 3, and the noise window width m/z was 250. The threshold after S/N recalculation was set at 20. The peptide fragments were assigned based on the UCSF Protein Prospector's MS-Digest function (26).

RT-PCR. RNA was isolated from purified virions and subjected to RT-PCR using an RT-PCR kit (NEB) and the following set of primers. A 1,700-nt fragment of B1 RNA located between the 3′ tRNA-like structure (TLS) and a portion of rep-1a open reading frame (ORF) was amplified with a reverse primer (5′-^{3234}TGGTCTCTTTTAGAGATTTAC^{3014}-3′) and forward primer (5′-^{1534}CTGAAGAGGACTTATTC^{1543}-3′). Likewise, a 1,700- nt fragment of B2 RNA located between the 3′ TLS and a portion of rep-2a ORF was amplified with a reverse primer (5′-^{2865}TGGTCTCTTTTAGAGATTTAC^{2846}-3′) and a forward primer (5′-^{1149}CTATGGATGTCATGACT^{1165}-3′). A 650-nt fragment of MP ORF of B3 RNA located between nucleotide (nt) 92 and 1007 was amplified using a reverse primer (5′-^{92}ATGTCTAACATAGTTTCTC^{110}-3′) and a forward primer (5′-^{752}CAGTCTGTCAAATGGCAT^{760}-3′). Similarly, a 650-nt fragment of CP ORF of B3/sgB4 RNA located between the 3′ TLS and a portion of the CP ORF was amplified with a reverse primer

(5′-²¹¹⁷TGGTCTCTTTTAGAGATTTAC¹⁹⁹⁷-3′) and a forward primer (5′-¹⁴⁵¹CATGAGTATCACTCTGC¹⁴³⁵-3′). The resulting PCR products were analyzed by electrophoresis in a 1% agarose gel.

REFERENCES

1. Mateu MG. 2013. Assembly, stability and dynamics of virus capsids. Arch Biochem Biophys 531:65–79. https://doi.org/10.1016/j.abb.2012.10.015.
2. Rao AL. 2006. Genome packaging by spherical plant RNA viruses. Annu Rev Phytopathol 44:61–87. https://doi.org/10.1146/annurev.phyto.44.070505.143334.
3. Johnson JE. 2003. Virus particle dynamics. Adv Protein Chem 64:197–218. https://doi.org/10.1016/s0065-3233(03)01005-2.
4. Rao A, Chaturvedi S, Garmann RF. 2014. Integration of replication and assembly of infectious virions in plant RNA viruses. Curr Opin Virol 9:61–66. https://doi.org/10.1016/j.coviro.2014.09.008.
5. Rao AL, Cheng Kao C. 2015. The brome mosaic virus 3′ untranslated sequence regulates RNA replication, recombination, and virion assembly. Virus Res 206:46–52. https://doi.org/10.1016/j.virusres.2015.02.007.
6. Kao CC, Sivakumaran K. 2000. Brome mosaic virus, good for an RNA virologist's basic needs. Mol Plant Pathol 1:91–97. https://doi.org/10.1046/j.1364-3703.2000.00017.x.
7. Miller WA, Dreher TW, Hall TC. 1985. Synthesis of brome mosaic virus subgenomic RNA in vitro by internal initiation on (-)-sense genomic RNA. Nature 313:68–70. https://doi.org/10.1038/313068a0.
8. Lane LC. 1981. Bromoviruses, p 333–376. In Kurstak E (ed), Hand book of plant virus infections and comparative diagnosis. Elsevier Biomedical Press, Amsterdam, Netherlands.
9. Lucas RW, Larson SB, McPherson A. 2002. The crystallographic structure of brome mosaic virus. J Mol Biol 317:95–108. https://doi.org/10.1006/jmbi.2001.5389.
10. Bamunusinghe D, Chaturvedi S, Seo JK, Rao AL. 2013. Mutations in the capsid protein of brome mosaic virus affecting encapsidation eliminate vesicle induction in planta: implications for virus cell-to-cell spread. J Virol 87:8982–8992. https://doi.org/10.1128/JVI.01253-13.
11. Rao AL, Grantham GL. 1995. Biological significance of the seven amino-terminal basic residues of brome mosaic virus coat protein. Virology 211:42–52. https://doi.org/10.1006/viro.1995.1377.
12. Schmitz I, Rao AL. 1996. Molecular studies on bromovirus capsid protein. I. Characterization of cell-to-cell movement-defective RNA3 variants of brome mosaic virus. Virology 226:281–293. https://doi.org/10.1006/viro.1996.0656.
13. Ni P, Vaughan RC, Tragesser B, Hoover H, Kao CC. 2014. The plant host can affect the encapsidation of brome mosaic virus (BMV) RNA: BMV virions are surprisingly heterogeneous. J Mol Biol 426:1061–1076. https://doi.org/10.1016/j.jmb.2013.09.007.
14. Vaughan R, Tragesser B, Ni P, Ma X, Dragnea B, Kao CC. 2014. The tripartite virions of the brome mosaic virus have distinct physical properties that affect the timing of the infection process. J Virol 88:6483–6491. https://doi.org/10.1128/JVI.00377-14.
15. Annamalai P, Rao AL. 2005. Replication-independent expression of genome components and capsid protein of brome mosaic virus in planta: a functional role for viral replicase in RNA packaging. Virology 338:96–111. https://doi.org/10.1016/j.virol.2005.05.013.
16. Annamalai P, Rao AL. 2006. Packaging of brome mosaic virus subgenomic RNA is functionally coupled to replication-dependent transcription and translation of coat protein. J Virol 80:10096–10108. https://doi.org/10.1128/JVI.01186-06.
17. Annamalai P, Rofail F, Demason DA, Rao AL. 2008. Replication-coupled packaging mechanism in positive-strand RNA viruses: synchronized co-expression of functional multigenome RNA components of an animal and a plant virus in Nicotiana benthamiana cells by agroinfiltration. J Virol 82:1484–1495. https://doi.org/10.1128/JVI.01540-07.
18. Chaturvedi S, Rao AL. 2014. Live cell imaging of interactions between replicase and capsid protein of Brome mosaic virus using bimolecular fluorescence complementation: implications for replication and genome packaging. Virology 464–465:67–75. https://doi.org/10.1016/j.virol.2014.06.030.
19. Bothner B, Dong XF, Bibbs L, Johnson JE, Siuzdak G. 1998. Evidence of viral capsid dynamics using limited proteolysis and mass spectrometry. J Biol Chem 273:673–676. https://doi.org/10.1074/jbc.273.2.673.
20. Calhoun SL, Rao AL. 2008. Functional analysis of brome mosaic virus coat protein RNA-interacting domains. Arch Virol 153:231–245. https://doi.org/10.1007/s00705-007-1085-z.
21. Calhoun SL, Speir JA, Rao AL. 2007. In vivo particle polymorphism results from deletion of a N-terminal peptide molecular switch in brome mosaic virus capsid protein. Virology 364:407–421. https://doi.org/10.1016/j.virol.2007.03.034.
22. Carrillo-Tripp M, Shepherd CM, Borelli IA, Venkataraman S, Lander G, Natarajan P, Johnson JE, Brooks CL, III, Reddy VS. 2009. VIPERdb2: an enhanced and web API enabled relational database for structural virology. Nucleic Acids Res 37:D436–D442. https://doi.org/10.1093/nar/gkn840.
23. Rayaprolu V, Kruse S, Kant R, Movahed N, Brooke D, Bothner B. 2014. Fluorometric estimation of viral thermal stability. Bio Protoc 4:e1199. https://doi.org/10.21769/bioprotoc.1199.
24. Bothner B, Schneemann A, Marshall D, Reddy V, Johnson JE, Siuzdak G. 1999. Crystallographically identical virus capsids display different properties in solution. Nat Struct Biol 6:114–116. https://doi.org/10.1038/5799.
25. Speir JA, Bothner B, Qu C, Willits DA, Young MJ, Johnson JE. 2006. Enhanced local symmetry interactions globally stabilize a mutant virus capsid that maintains infectivity and capsid dynamics. J Virol 80:3582–3591. https://doi.org/10.1128/JVI.80.7.3582-3591.2006.
26. Running WE, Ni P, Kao CC, Reilly JP. 2012. Chemical reactivity of brome mosaic virus capsid protein. J Mol Biol 423:79–95. https://doi.org/10.1016/j.jmb.2012.06.031.
27. Zlotnick A, Aldrich R, Johnson JM, Ceres P, Young MJ. 2000. Mechanism of capsid assembly for an icosahedral plant virus. Virology 277:450–456. https://doi.org/10.1006/viro.2000.0619.
28. Zhao X, Fox JM, Olson NH, Baker TS, Young MJ. 1995. In vitro assembly of cowpea chlorotic mottle virus from coat protein expressed in Escherichia coli and in vitro-transcribed viral cDNA. Virology 207:486–494. https://doi.org/10.1006/viro.1995.1108.
29. Okinaka Y, Mise K, Suzuki E, Okuno T, Furusawa I. 2001. The C terminus of brome mosaic virus coat protein controls viral cell-to-cell and long-distance movement. J Virol 75:5385–5390. https://doi.org/10.1128/JVI.75.11.5385-5390.2001.
30. Kaper JM. 1973. Arrangement and identification of simple isometric viruses according to their dominating stabilizing interactions. Virology 55:299–304. https://doi.org/10.1016/s0042-6822(73)81035-9.

31. Lane LC. 1974. The bromoviruses. Adv Virus Res 19:151–220. https://doi .org/10.1016/s0065-3527(08)60660-0.

32. Hull R. 1976. The behavior of salt-labile plant viruses in gradients of cesium sulphate. Virology 75:18–25. https://doi.org/10.1016/0042-6822 (76)90003-9.

33. Ahlquist P. 1992. Bromovirus RNA replication and transcription. Curr Opin Genet Dev 2:71–76. https://doi.org/10.1016/s0959-437x(05)80325-9.

34. Bamunusinghe D, Seo JK, Rao AL. 2011. Subcellular localization and rearrangement of endoplasmic reticulum by Brome mosaic virus capsid protein. J Virol 85:2953–2963. https://doi.org/10.1128/JVI.02020-10.

35. Schwartz M, Chen J, Lee WM, Janda M, Ahlquist P. 2004. Alternate, virus-induced membrane rearrangements support positive-strand RNA virus genome replication. Proc Natl Acad Sci U S A 101:11263–11268. https://doi.org/10.1073/pnas.0404157101.

36. de Wispelaere M, Sivanandam V, Rao A. 2020. Regulation of positive-strand accumulation by capsid protein during brome mosaic virus infection in planta. Phytopathology 110:228–236. https://doi.org/10.1094/ PHYTO-07-19-0236-FI.

37. Ni P, Cheng Kao C. 2013. Non-encapsidation activities of the capsid proteins of positive-strand RNA viruses. Virology 446:123–132. https:// doi.org/10.1016/j.virol.2013.07.023.

38. Galaz-Montoya JG, Flanagan J, Schmid MF, Ludtke SJ. 2015. Single particle tomography in EMAN2. J Struct Biol 190:279–290. https://doi .org/10.1016/j.jsb.2015.04.016.

39. Galaz-Montoya JG, Ludtke SJ. 2017. The advent of structural biology. Biophys Rep 3:17–35. https://doi.org/10.1007/s41048-017-0040-0.

40. Seo JK, Kwon SJ, Rao AL. 2012. A physical interaction between viral replicase and capsid protein is required for genome-packaging specificity in an RNA virus. J Virol 86:6210–6221. https://doi.org/10.1128/JVI.07184-11.

41. Rao ALN, Duggal R, Lahser FC, Hall TC. 1994. Analysis of RNA replication in plant viruses, p 216–236. In Adolph KW (ed), Methods in molecular genetics: molecular virology techoiques, vol 4. Academic Press, San Diego, CA.

42. Schneider CA, Rasband WS, Eliceiri KW. 2012. NIH Image to ImageJ: 25 years of image analysis. Nat Methods 9:671–675. https://doi.org/10 .1038/nmeth.2089.